Journal of
Polymer Materials

Tech Science Press

https://doi.org/10.32604/jpm.2026.081661

ARTICLE

Co-Encapsulation of Silymarin and Mesenchymal Stromal Cells in PEG Norbornene Microgels Enhances HepG2 Cell Resistance to Inflammatory Damage

Zhihuan Li[1,#], Shiqi Lei[1,#], Yajuan Guo[1], Renmeng Liu[1], Lei Yang[1], Yuheng Du[1], Xingdan Wang[1], Yun Zou[2,*], Kun Jiang[1,*] and Zhongliang Jiang[1,*]

[1]School of Chemical Engineering, University of Science and Technology Liaoning, Anshan, China
[2]Department of Stomatology, Ansteel General Hospital, Anshan, China

*Corresponding Authors: Yun Zou. Email: zouyun5545133@126.com; Kun Jiang. Email: 322201@ustl.edu.cn; Zhongliang Jiang. Email: jz82070@163.com

[#]These authors contributed equally to this work

Received: 06 March 2026; Accepted: 03 June 2026; Published: 30 June 2026

ABSTRACT: Inflammatory liver injury represents a significant clinical challenge, characterized by a hostile immune microenvironment and extensive tissue damage. Although silymarin and mesenchymal stromal cells (MSCs) show promise in treating inflammatory liver injury, their efficacy is restricted by the drug's poor bioavailability while MSC therapy is hampered by low cellular viability under inflammatory stress. To overcome these challenges, we engineered a droplet-microfluidic-assisted platform to co-encapsulate silymarin and MSCs within uniform, biocompatible polyethylene glycol-norbornene (PEGNB) hydrogel microspheres. This design establishes a dual-functional scaffold that supports MSC survival by shielding them from the harsh milieu while enabling the sustained, localized release of silymarin. Crucially, we elucidate a synergistic mechanism wherein the sustained release of silymarin modulates the local microenvironment, and augmenting the paracrine activity of the co-encapsulated MSCs. This synergy is significantly supported by a marked elevation in the expression of anti-inflammatory factors, including Interleukin-10 (IL-10) and Transforming Growth Factor-β (TGF-β). Establishing an indirect co-culture via transwell inserts, we demonstrate that this bio-functionalized platform significantly mitigates Lipopolysaccharide (LPS)-induced damage in HepG2 cells by suppressing pro-inflammatory cytokines, including Tumor Necrosis Factor-α (TNF-α) and Interleukin-6 (IL-6), while preserving hepatocyte metabolic stability against inflammatory stress. This high-throughput strategy offers a promising approach to modulate pathological stress microenvironments, driving advancements in precision regenerative medicine.

KEYWORDS: Droplet-microfluidics; PEGNB microgels; MSCs; silymarin; hepatoprotection; sustained release

1 Introduction

Inflammatory liver diseases, including viral and drug-induced hepatitis, are primarily driven by dysregulated immune responses and oxidative stress [1,2]. Central to this pathology is the activation of Kupffer cells and monocytes, which inundate the hepatic microenvironment with a cytokine storm dominated by TNF-α and IL-6 [2–4]. TNF-α acts as a master initiator of the inflammatory cascade by binding to specific receptors on hepatocytes and hepatic stellate cells, it activates downstream signaling pathways—most notably nuclear factor kappa-light-chain-enhancer of activated B cells (NF-κB) and mitogen-activated protein kinase

(MAPK) [5]. This activation not only induces the production of further pro-inflammatory mediators but also amplifies the hepatic inflammatory response [6,7]. This inflammatory milieu is further exacerbated by IL-6, lowering the threshold for TNF-α-induced hepatocyte apoptosis and thereby stifling the liver's innate regenerative capacity [8,9]. Persistent NF-κB signaling amplifies the transcription of inflammatory mediators and adhesion molecules, aggravating hepatic injury [5]. Additionally, excessive reactive oxygen species (ROS) generation induces endoplasmic reticulum (ER) stress and mitochondrial dysfunction, resulting in apoptosis and impaired hepatocyte regeneration [10–13].

The co-delivery of hepatoprotective agents and therapeutic cells holds true promise as a comprehensive strategy to achieve liver protection. MSCs have emerged as a potent therapeutic candidate due to their intrinsic immunomodulatory properties and their ability to secrete trophic factors that support tissue repair [14–16]. Specifically, MSCs secrete anti-inflammatory cytokines such as IL-10 and TGF-β, along with regenerative growth factors [17]. IL-10 serves as a master regulator of the inflammatory microenvironment. It functions not only by directly blocking the NF-κB signaling cascade to suppress pro-inflammatory cytokines, but also by driving the phenotypic polarization of local macrophages from a pro-inflammatory M1 state towards a reparative M2 phenotype, thereby actively resolving inflammation [18]. Additionally, TGF-β operates through canonical Smad-dependent signaling pathways to orchestrate tissue reconstruction. Beyond its role in immune tolerance, TGF-β is pivotal for upregulating the expression of essential extracellular matrix proteins and growth factors, thus facilitating the structural regeneration of the injured hepatic niche [19]. However, the efficacy of MSCs is heavily influenced by the surrounding microenvironment [14,20,21]. Silymarin, a flavonoid extracted from *Silybum marianum*, is widely recognized for its hepatoprotective effects [22–25]. Notably, recent investigations have illuminated that silybin, the major active constituent of silymarin, can function as a synergistic enhancer for MSCs, effectively augmenting their immunoregulatory efficacy by modulating inflammatory signaling pathways and suppressing downstream cytokine release (e.g., TNF-α, IL-6) [14,21,26]. Furthermore, silymarin has been shown to promote the proliferation and inhibit the apoptosis of MSCs to a certain extent [27]. Silybin also protected hepatocytes via its antioxidant property, improving the microenvironment of the damaged liver. This optimization promoted the homing and survival of transplanted MSCs [28]. This suggests that combining these two agents could offer superior therapeutic outcomes compared to monotherapies.

However, the clinical translation of this combined approach is hindered by the intrinsic limitations of conventional delivery methods. Silymarin suffers from low bioavailability due to its poor aqueous solubility and rapid metabolism, meaning that systemic administration often fails to maintain effective local concentrations [29]. Additionally, the direct transplantation of MSCs alone is equally inefficient. Lacking extracellular matrix support, suspended MSCs rapidly undergo anoikis [30,31]. Furthermore, without physical shielding, the transplanted cells are susceptible to hemodynamic circulation and are immediately besieged by the hostile ROS-enriched inflammatory milieu [13]. High levels of TNF-α and IL-6 readily trigger inflammation-mediated apoptosis, leading to poor cell retention and impaired therapeutic function [32]. Consequently, to harness the full synergistic potential, there is a critical need for an engineered vehicle that can simultaneously function as a sustained drug reservoir and a protective niche—preventing anoikis and insulating MSCs from the harsh microenvironment. Establishing such a protective niche is critical, as the therapeutic efficacy of MSCs relies heavily on their ability to secrete specific immunomodulatory factors [33]. However, in conventional therapies, this secretory function is rapidly lost as transplanted cells die or lose their native 3D support [34,35].

We therefore hypothesize that the 3D environment of the microgels, combined with the support from co-encapsulated silymarin, can synergistically sustain and even enhance the secretion of these vital

factors [36]. To address these limitations, we introduced droplet microfluidics and PEGNB hydrogel. PEG-based hydrogels typically exhibit minimal immunogenicity and inherent biological inertness [37]. As a high-throughput platform, droplet microfluidics enables the co-encapsulation of cells and drugs, facilitating the precise formation of microgels for integrated therapeutic delivery and cellular studies [38]. In the present work, this platform was constructed using polydimethylsiloxane (PDMS), a flexible and readily moldable material that has also been widely adopted in a variety of functional biomedical devices [39,40]. Furthermore, PEGNB exhibits superior biocompatibility and other unique physicochemical properties, rendering it a more suitable candidate for cell encapsulation [41–44]. Through thiol-ene photoclick chemistry, PEGNB allows for rapid, cytocompatible gelation suitable for on-chip microfluidic encapsulation [45,46], offering a tunable mesh size that permits the diffusion of therapeutic factors while protecting cells from harsh external stimuli [42]. MSCs encapsulated in PEGNB microgels maintained high viability and exhibited enhanced trophic factor expression, with conditioned media significantly promoting fibroblast migration and proliferation [39,47]. Meanwhile, the tunable mesh size enables the sustained release of silymarin particles, thereby enhancing the overall therapeutic efficacy. Coupled with droplet-microfluidic technology, this system ensures the high-throughput generation of highly monodisperse microgels with precise control over cell loading and drug encapsulation efficiency [48,49].

In this study, we co-encapsulated MSCs and silymarin within PEGNB microgels fabricated by droplet microfluidics, establishing a novel co-delivery strategy that integrates both pharmacological agents and cellular components (Fig. 1). This design was used to establish a dual-functional scaffold: the PEGNB matrix serves as a 3D protective shield that supports quantitative MSC survival, while simultaneously acting as a sustained-release vehicle to ensure high local concentrations of silymarin. Subsequently, the therapeutic efficacy of the co-encapsulated microgels was systematically evaluated using an *in vitro* hepatic inflammation model induced by LPS stimulation of HepG2 cells [50]. By monitoring cell viability and the expression of crucial inflammatory cytokines (TNF-α, IL-6), we demonstrate that this engineering strategy not only addresses the bioavailability limitations highlighted in recent studies but also amplifies the synergistic hepatoprotective effects of MSCs and silymarin. The development of this cell-drug co-encapsulation strategy offers a promising and robust platform for modulating the inflammatory microenvironment in liver injury repair.

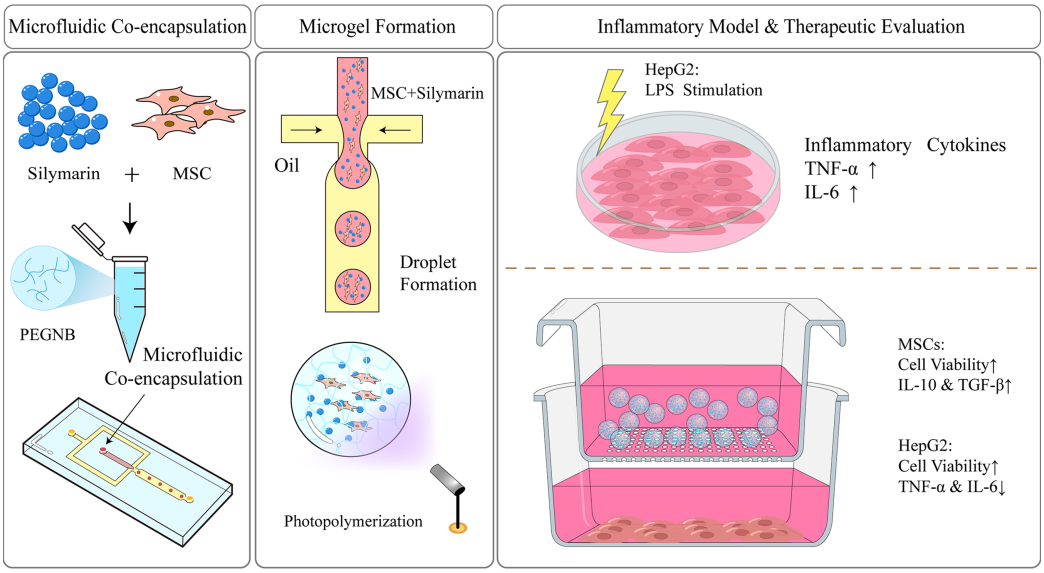

Figure 1: Schematic illustration of the engineered microfluidic platform for synergistic hepatoprotection. The strategy involves (Left) the preparation of the aqueous phase containing PEGNB, photoinitiator (LAP), Silymarin, and MSCs,

(Continued)

Figure 1: (continued) followed by injection into a flow-focusing microfluidic device. (Middle) The generation of monodisperse cell-drug laden droplets and subsequent UV photopolymerization to form stable hydrogel microspheres. (Right) The establishment of an *in vitro* therapeutic evaluation model using a Transwell co-culture system. The dual-functional microgels synergistically mitigate LPS-induced inflammatory damage in HepG2 cells by enabling the sustained release of Silymarin and enhancing MSCs paracrine function (upregulation of IL-10 and TGF-β), resulting in the suppression of pro-inflammatory cytokines (TNF-α and IL-6) and the restoration of hepatocyte viability.

2 Materials and Methods

2.1 Optimization and Quantification of Silymarin Extraction

Silymarin was extracted from the seeds of *Silybum marianum* using a modified ethanol reflux technique. To determine the optimal extraction conditions, an orthogonal experimental design was employed. Three key variables—ethanol concentration (70%, 80%, 90%), solid-liquid ratio (1:8, 1:10, 1:12 w/v), and extraction time (0.5, 1.0, 1.5 h)—were investigated. Briefly, pulverized seeds were suspended in ethanol solution according to the experimental design, soaked for 15 min, and subjected to reflux extraction. Based on the optimization results, the final extraction was performed using 80% ethanol with a solid-liquid ratio of 1:12 for 0.5 h. The supernatant was filtered, incubated at −80°C overnight to precipitate lipids, and concentrated to dryness.

For chemical characterization, the dried silymarin extract was re-dissolved in ethanol. As Silybin is the major active constituent of silymarin, it was selected as the marker compound for quantification. High-Performance Liquid Chromatography (HPLC) analysis was performed on an Agilent 1100 system (Agilent Technologies, Santa Clara, CA, USA) equipped with a binary pump, an autosampler, and a diode array detector (DAD). Chromatographic separation was carried out on a Dikma Diamonsil C18 (2) column (150 mm × 4.6 mm, 5 μm; Dikma Technologies, Beijing, China). The mobile phase consisted of an isocratic mixture of methanol and deionized water (50:50, v/v) delivered at a constant flow rate of 0.6 mL/min and the injection volume was 3 μL. The column temperature was maintained at 35°C, and absorbance was monitored at 280 nm. The total content of Silybin was determined by summing the peak areas of its two diastereoisomers (Silybin A and Silybin B). Quantification was performed using the external standard method based on a calibration curve established with a commercial Silybin standard (Macklin, Shanghai, China). The silymarin stock solution was prepared in phosphate-buffered saline (PBS, pH 7.4, Biosharp, Hefei, China), subjected to sonication for 30 min with shaking, and subsequently quantified by HPLC. For HPLC quantification, nine volumes of ethanol were added to the sample to obtain a final 90% (v/v) ethanol solution prior to analysis.

2.2 Cell Culture and In Vitro Inflammation Model Establishment

HepG2 cells and mouse MSCs were maintained in Low Glucose Dulbecco's Modified Eagle's Medium (DMEM; Biosharp, China), both media were supplemented with 10% fetal bovine serum (FBS; Biosharp, China) and 1% antibiotic-antimycotic solution (Biosharp, China). Cells were incubated at 37°C in a humidified atmosphere containing 5% CO_2.

To establish the *in vitro* inflammation model, HepG2 cells were seeded in culture plates. After cell attachment, the culture medium was replaced with fresh medium containing LPS (1 μg/mL, Biosharp, China). The cells were stimulated with LPS (1 μg/mL) for 24 h to induce the expression of pro-inflammatory cytokines. This protocol was established to capture the critical window of peak transcriptional upregulation for inflammatory markers (TNF-α, IL-6), aligning with standardized models that demonstrate signal attenuation during prolonged exposure (e.g., 72 h) [51]. Furthermore, the selected concentration ensures a robust and consistent inflammatory response, as validated in kinetic studies of HepG2 sensitivity [52,53].

All instruments and materials used in this experiment were sterilized by autoclaving where appropriate or obtained as sterile products, and all procedures were performed using aseptic techniques.

2.3 Cytotoxicity Assessment of Free Silymarin

For the identification of a safe dosage for future tests, the viability of MSCs and HepG2 cells exposed to free silymarin was systematically evaluated. Briefly, 96-well plates were seeded with cells at 1×10^4 cells per well and cultured at 37°C for 24 h to allow attachment. Subsequently, cells were treated with various concentrations of silymarin to achieve final concentrations of 5, 10, 15, 20, 25, 30, 40, and 60 μg/mL. The silymarin stock solution was dissolved in DMSO, and the final concentration of DMSO in the culture medium was maintained below 0.1% (v/v) in all groups to minimize solvent cytotoxicity. After 24 h of exposure, cell viability was quantified using an MTT Cell Proliferation and Cytotoxicity Assay Kit (Biosharp, China) in accordance with the supplier's protocol, and the resulting optical densities were recorded on a BioTek PowerWave HT Microplate Reader (BioTek Instruments, USA).

2.4 Fabrication and Operation of Droplet-Microfluidic Device

Microfluidic devices were fabricated using standard soft lithography techniques. Briefly, PDMS (Sylgard 184, Dow Corning, USA) elastomer and curing agent were mixed, degassed, and poured onto a silicon wafer patterned with SU-8 photoresist (MicroChem, Winooski, VT, USA). After curing at 70°C for 4 h, the PDMS replicas were peeled off, punched with a 0.75 mm biopsy punch to create inlets and outlets, and bonded to glass slides following oxygen plasma treatment (Harrick Plasma, Ithaca, NY, USA). The microchannels were treated with Aquapel (PPG Industries, Pittsburgh, PA, USA) to render the surfaces hydrophobic.

2.5 In Vitro Drug Release Kinetics Profile

To evaluate the drug release capability of the PEGNB microgels, the total drug loading was first calculated. The concentration of the initial silymarin solution was determined by HPLC, and the silymarin concentration in the hydrogel-forming solution was calculated accordingly during preparation. For the release study, an equal amount of microgels was suspended in 1 mL of PBS in a release vial and incubated at 37°C with gentle shaking (40 rpm). At predetermined time intervals (1, 3, 6, 12, 24, 48, 72, 96, 120, 144, and 168 h), the entire supernatant was collected and replaced with fresh buffer. Following sample collection, the amount of liberated silymarin was determined using the HPLC methodology outlined in Section 2.1. These measurements were then utilized to calculate the cumulative release fraction based on the previously determined total drug encapsulation.

2.6 Microfluidic Co-Encapsulation of MSCs and Silymarin

The precursor solution was prepared by mixing 20 wt% PEGNB (MW 10 kDa; JenKem Technology, Beijing, China), 100 mm PEG-dithiol crosslinker (MW 3.4 kDa; JenKem Technology), and 3 wt% photoinitiator lithium acylphosphinate salt (LAP; Sigma-Aldrich, St. Louis, MO, USA) with a specific amount of silymarin solution and MSC suspension to yield final concentrations of 5 wt% PEGNB, 10 mm PEG-dithiol crosslinker, and 0.1 wt% LAP.

The oil phase consisted of Novec 7500 fluorinated oil (3M, St. Paul, MN, USA) containing 2 wt% surfactant (Pico-Surf 1, Sphere Fluidics, Cambridge, UK). The aqueous and oil phases were injected into the microfluidic device at flow rates of 5 μL/min and 25 μL/min, respectively, using syringe pumps. At the flow-focusing junction, the continuous oil phase sheared the aqueous precursor stream into discrete droplets; the oil phase was also required to enable droplet pinch-off, prevent coalescence, and maintain

droplet stability prior to photopolymerization. The generated droplets were photocrosslinked by exposure to UV light (365 nm, 100 mW/cm^2) for 20 s.

2.7 Analysis of Encapsulated MSC Viability

Cell survival within the microgels was monitored on the first and seventh days following encapsulation via a commercial Live/Dead Viability Kit (Life Technologies, Carlsbad, CA, USA). Briefly, microgels were incubated with calcein-AM (2 μM) and ethidium homodimer-1 (4 μM) for 30 min at room temperature. Live cells (green fluorescence) and dead cells (red fluorescence) were visualized using an inverted fluorescence microscope (IX-71, Olympus, Center Valley, PA, USA). Live/dead cell staining is based on differences in membrane integrity, utilizing specific fluorescent dyes to distinguish viable cells from non-viable ones [54–56]. Finally, the quantitative viability rate was determined via ImageJ by dividing the number of live cells by the total cell population, based on observations of at least 50 randomly selected microgels per condition.

2.8 Indirect Transwell Co-Culture System

A Transwell system (0.4 μm pore size, Biosharp, China) was utilized to evaluate the therapeutic efficacy of the microgels. HepG2 cells (2×10^5 cells/well) were seeded in the lower reservoir (24-well plate) and stimulated with LPS (1 μg/mL, Biosharp, China) for 24 h to induce inflammation. Subsequently, the co-encapsulated microgels were transferred into the upper inserts. The co-culture system was incubated for 24 h.

2.9 Gene Expression Analysis of Paracrine and Inflammatory Factors by RT-qPCR

Total RNA was extracted from the MSCs and HepG2 cells using Trizol reagent (Biosharp, China) according to the manufacturer's instructions. The concentration and purity of the isolated RNA were assessed using a NanoDrop spectrophotometer (Thermo Fisher Scientific, Waltham, MA, USA).

Subsequently, cDNA was synthesized from 1 μg of the extracted RNA using the First Strand cDNA Synthesis Kit (Biosharp, China) on an Applied Biosystems Veriti 96-Well Thermal Cycler (Applied Biosystems, Waltham, MA, USA). And, qPCR was conducted using Universal SYBR qPCR Master Mix (Biosharp, China) and a Bio-Rad CFX96 Real-Time System (Bio-Rad, Hercules, CA, USA). The amplification protocol consisted of an initial denaturation at 95°C for 2 min, followed by 40 cycles of 95°C for 15 s and 60°C for 30 s. The relative gene expression levels were calculated using the $2^{-\Delta\Delta Ct}$ method, with GAPDH (for HepG2 cells) and β-actin (for MSCs) serving as internal reference genes for normalization. All primer sequences, synthesized by Sangon Biotech (Shanghai, China), are detailed in Table 1.

Table 1: Primer sequences used for RT-qPCR.

Species	Gene	Forward Primer (5′-3′)	Reverse Primer (5′-3′)
Human	TNF-α	CCTCTCTCTAATCAGCCCTCTG	GAGGACCTGGGAGTAGATGAG
	IL-6	GGCACTGGCAGAAAACAACC	GCAAGTCTCCTCATTGAATCC
	GAPDH	AGGTCGGTGTGAACGGATTTG	TGTAGACCATGTAGTTGAGGTCA
Mouse	IL-10	AAGGCAGTGGAGCAGGTGAA	CCAGCAGACTCAATACACAC
	TGF-β1	TGAACCAAGGAGACGGAATACAGG	GCCATGAGGAGCAGGAAGGG
	β-actin	GATTACTGCTCTGGCTCCTA	ATCGTACTCCTGCTTGCTGA

2.10 Statistical Analysis

We report all quantitative values as the mean ± standard deviation (SD) based on at least three separate experiments. GraphPad Prism software was utilized for all statistical processing. We assessed group differences using a one-way analysis of variance (ANOVA) coupled with Tukey's multiple comparison test, defining statistical significance as $p < 0.05$.

3 Results and Discussion

3.1 Extraction and Identification of Silymarin

To optimize the extraction process, the efficiency of silymarin recovery was evaluated across various concentrations of ethanol as the extraction solvent. The optimal ethanol concentration for silymarin extraction was found to be 80%; furthermore, elevating the solid-liquid ratio significantly boosted the overall yield (Fig. 2A). Subsequent experiments were conducted under these optimized conditions of solvent concentration and solid-liquid ratio. Meanwhile, Prolonging the extraction duration did not further enhance the silymarin yield, as the majority of the compound was successfully recovered from the seeds within the initial 30 min. By comparing the chromatograms with the standard silybin sample, the retention times for silybin A and B were identified at approximately 12.6 and 14.8 min, respectively (Fig. 2C,D).

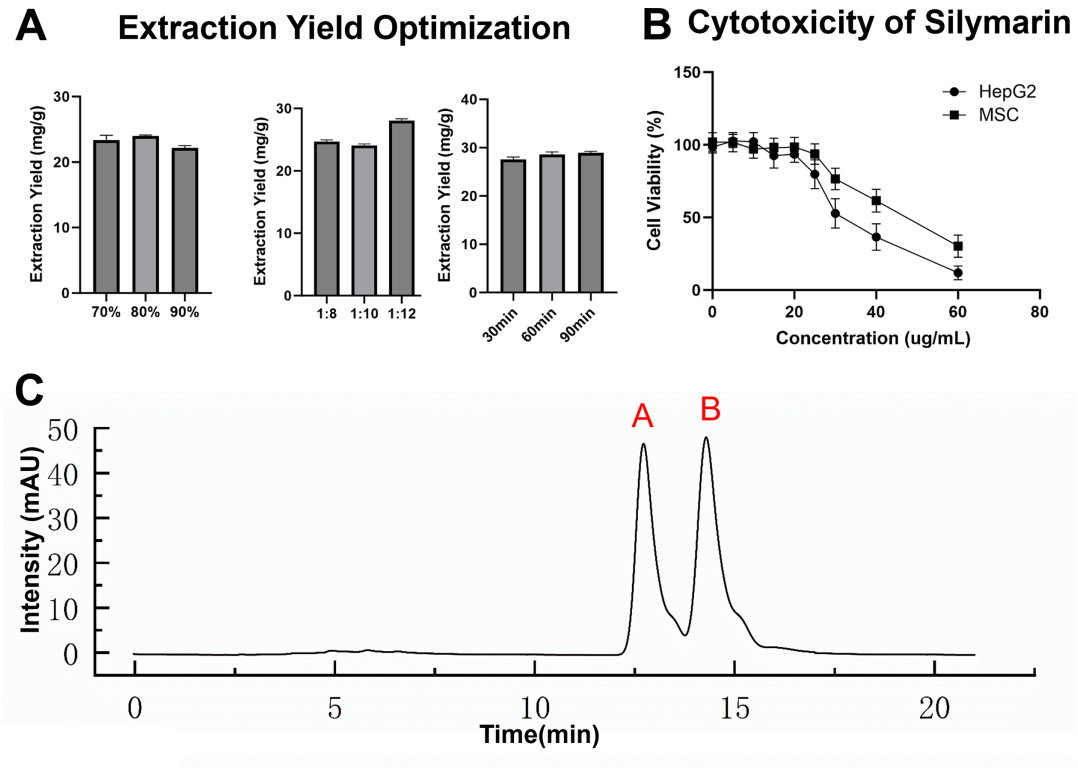

Figure 2: (Continued)

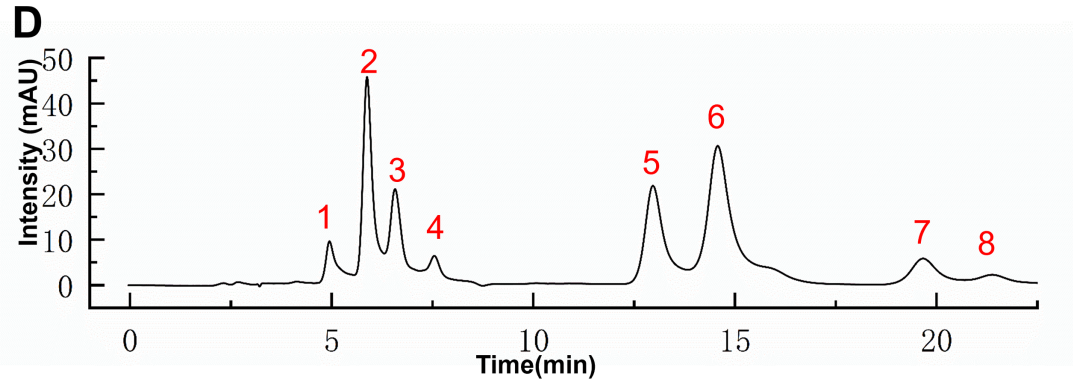

Figure 2: Extraction optimization, characterization, and release kinetics of Silymarin. (**A**) The effects of ethanol concentration, solid-liquid ratio, and extraction time on the Silymarin extraction yield (mg/g) were systematically evaluated to determine the optimal parameters. (**B**) *In vitro* cytotoxicity assessment (dose-response) of free Silymarin (dissolved in DMSO, final concentration <0.1% v/v) on HepG2 cells and MSCs determined by MTT assay. The results establish the safe dosage range for co-encapsulation, showing high MSCs tolerance compared to HepG2 sensitivity. (**C**) Representative HPLC chromatogram of standard silymarin, where peak A corresponds to silybin A and peak B corresponds to silybin B. (**D**) Representative HPLC chromatogram of the purified silymarin extract. The numbered peaks correspond to the following compounds: 1 = taxifolin, 2 = silychristin, 3 = apigenin 7-glucoside, 4 = silydianin, 5 = silybin A, 6 = silybin B, 7 = isosilybin A, and 8 = isosilybin B. Data are presented as mean ± SD (n = 3).

3.2 Cytotoxicity Evaluation of Silymarin

Establishing a safe dosage window is critical prior to encapsulation. We therefore evaluated the cytotoxicity of silymarin on both HepG2 cells and MSCs (Fig. 2B). Both cell types exhibited a dose-dependent response; however, at 20 μg/mL, silymarin exhibited negligible cytotoxicity towards both HepG2 cells and MSCs. Based on this balance, 20 μg/mL was selected as the working concentration. Furthermore, the toxicity observed at high silymarin concentrations is non-specific; rather than triggering specific programmed cell death, it results from non-specific cellular damage induced by excessive dosage.

3.3 In Vitro Release Kinetics of Silymarin-Loaded Microgels

The silymarin-loaded PEGNB microgels fabricated by droplet microfluidics exhibited a uniform spherical morphology (Fig. 3A). The *in vitro* release profile exhibits a distinct controlled-release pattern, characterized by an initial release of approximately 40% silymarin within the first 24 h, followed by a sustained and gradual increase reaching approximately 75% by the 72-h time point and approximately 88% at 168 h (7 days) (Fig. 3B).

3.4 Cytocompatibility and Sustained Viability of Encapsulated MSCs

Verifying the cytocompatibility of the microfluidic process and the PEGNB matrix is a prerequisite. We utilized a Live/Dead staining assay to visualize MSC survival. Immediately following encapsulation (Day 1), the encapsulated MSCs exhibited robust green fluorescence with minimal red signals, indicating a high initial cell viability within the microgels (Fig. 3C). This high viability was maintained after 7 days of culture (Fig. 3D), indicating that the PEGNB network facilitates efficient nutrient transport. Quantitative analysis further confirmed this stability, with MSCs maintaining a robust average viability exceeding 90% throughout the culture period (Fig. 3E). Compared to our previously reported data on MSCs encapsulated alone, the viability of co-encapsulated MSCs remained comparable, showing no significant decline [47].

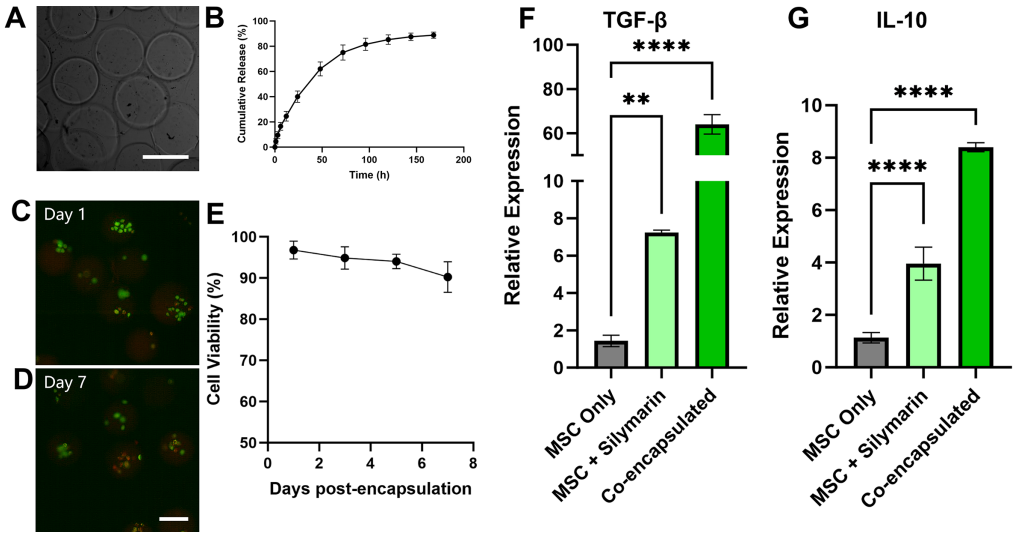

Figure 3: Cytocompatibility and enhanced paracrine function of MSCs within the co-encapsulated microenvironment. (**A**) Representative bright-field image of PEGNB microgels encapsulated with silymarin, demonstrating uniform morphology. Scale bar = 100 μm. (**B**) *In vitro* cumulative drug release profile of Silymarin from the PEGNB microgels in PBS (pH 7.4) containing 0.1% (v/v) DMSO at 37°C. The curve demonstrates a sustained release behavior without significant burst effect over 168 h. (**C**,**D**) Representative Live/Dead staining fluorescence images of MSCs encapsulated in PEGNB microgels at Day 1 (**C**) and Day 7 (**D**) (Green: live cells; Red: dead cells). The predominance of green fluorescence indicates minimal cytotoxicity during the microfluidic fabrication process. Scale bar = 100 μm. (**E**) Quantitative analysis of MSCs viability over 7 days in microgels co-encapsulated with silymarin, demonstrating that the cells maintained a robust survival rate exceeding 90% within this 3D hydrogel niche. (**F**,**G**) RT-qPCR analysis of therapeutic paracrine factors TGF-β (**F**) and IL-10 (**G**) expressed by MSCs. The Co-encapsulated group exhibited a significant upregulation of both anti-inflammatory factors compared to the MSCs Only and MSCs + Silymarin groups. Notably, the upregulation of TGF-β was more pronounced, suggesting that the sustained release of Silymarin synergistically potentiates MSCs secretory function. Data are presented as mean ± SD (n = 3). Statistical significance: $^{**}p < 0.01$, $^{****}p < 0.0001$.

3.5 Silymarin Modulates the Microenvironment and Enhances MSC Paracrine Function

We hypothesized that this sustained release would potentiate MSC functionality. To test this, we analyzed the expression of therapeutic factors. Compared to the moderate increase in TGF-β expression observed with free silymarin, the co-encapsulated group elicited a significantly more pronounced upregulation, highlighting its superior therapeutic efficacy (Fig. 3F). Similarly, IL-10 expression was most profoundly enhanced in the co-encapsulated group (Fig. 3G), reaching approximately 3.7-fold that of the control. These results suggest that the engineered microenvironment actively primes MSCs for enhanced therapeutic efficacy. Specifically, the co-encapsulation strategy—ensuring a sustained, high-concentration local drug supply within the 3D niche—amplifies the secretion of immunomodulatory factors significantly more than bolus drug administration.

3.6 Co-Encapsulated Microgels Mitigate Inflammatory Damage in HepG2 Cells via Transwell Co-Culture

Finally, to evaluate the therapeutic efficacy, we established an indirect Transwell co-culture system where LPS-challenged HepG2 cells in the lower reservoir were treated with different microgel formulations placed in the upper chamber (Fig. 1).

To confirm the anti-inflammatory mechanism, we analyzed the expression of pro-inflammatory markers, TNF-α and IL-6, in the treated HepG2 cells. RT-qPCR analysis revealed that LPS induction

triggered a drastic surge in both markers. This pronounced upregulation confirms that the 24 h interval effectively captures the acute inflammatory phase—characterized by concurrent oxidative stress and cytokine secretion—consistent with the kinetic profiles established in previous pharmacological investigations [51,52]. Notably, this time point is pivotal for assessing therapeutic efficacy, as extending the inflammatory challenge is known to result in the downregulation of these key cytokine signals [53]. Remarkably, co-culture with the dual-loaded microgels resulted in a significant and synergistic downregulation of TNF-α (Fig. 4A) and IL-6 (Fig. 4B), reducing their levels more effectively than either mono-therapy.

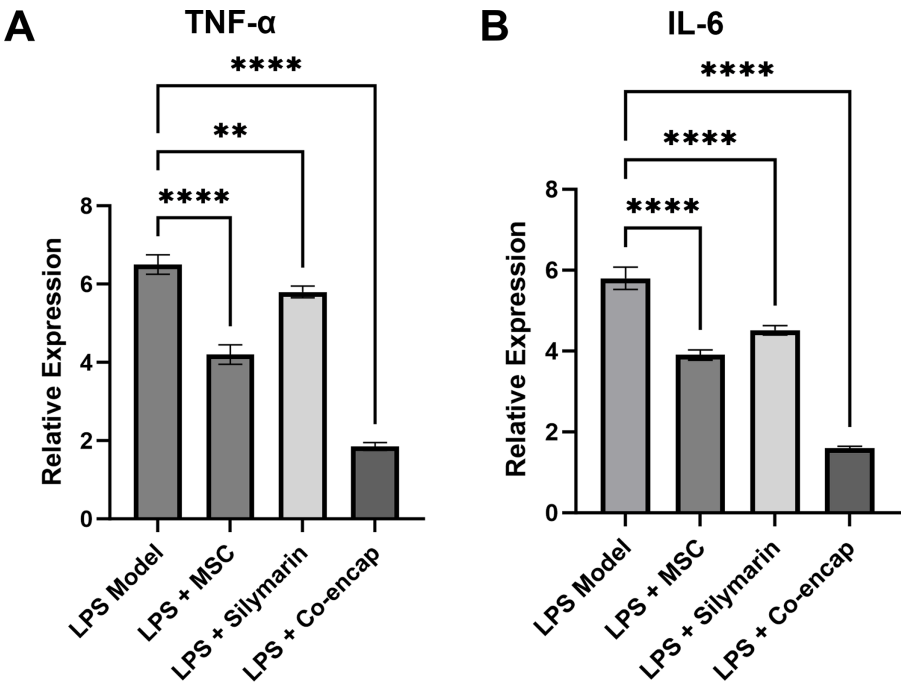

Figure 4: Synergistic anti-inflammatory efficacy in an LPS-induced HepG2 injury model. Assessment of mRNA levels for key pro-inflammatory targets, TNF-α (**A**) and IL-6 (**B**). Cells treated with the co-encapsulation microgels exhibited the strongest inhibition of these inflammatory indices, providing clear evidence for the platform's ability to downgrade the inflammatory response. Data are presented as mean ± SD (n = 3). Statistical significance: $^{**}p < 0.01$, $^{****}p < 0.0001$.

These results confirm that the continuous *in situ* delivery of silymarin and the enhanced secretion of MSC-derived factors work synergistically to quench the inflammatory cascade.

4 Conclusion

In summary, we have successfully engineered a droplet-microfluidic-assisted platform to co-encapsulate MSCs and silymarin within uniform, biocompatible PEGNB microgels. This strategy effectively addresses two critical challenges in current liver injury therapies: the poor bioavailability of hydrophobic hepatoprotective drugs and the rapid loss of MSC viability in harsh inflammatory microenvironment. By establishing a dual-functional scaffold, our system supports quantitative MSCs survival while enabling the sustained, localized release of silymarin.

Crucially, our findings elucidate a synergistic mechanism wherein the sustained delivery of silymarin modulates the local niche, significantly outperforming the direct administration of free drug in potentiating the paracrine function of the co-encapsulated MSCs. This synergy was evidenced by the marked upregulation of therapeutic factors (IL-10, TGF-β) and the subsequent potent suppression of pro-inflammatory

cytokines (TNF-α, IL-6) in an LPS-induced HepG2 injury model. Consequently, the engineered platform demonstrated superior efficacy in protecting hepatocytes from inflammatory damage compared to mono-therapeutic approaches. Collectively, this work establishes a robust and versatile strategy for cell-drug combination therapy, offering valuable insights into microenvironmental modulation for the precision treatment of inflammatory liver diseases.

Acknowledgement: Not applicable.

Funding Statement: This work was supported by the Liaoning Province Ph.D. Start-up Program (2023BS-183), and the University of Science and Technology Liaoning Excellent Young Faculty Program (2023YQ09).

Author Contributions: The authors confirm contribution to the paper as follows: study conception and design: Zhihuan Li, Zhongliang Jiang, Yun Zou; data collection: Zhihuan Li, Shiqi Lei; analysis and interpretation of results: Yun Zou, Zhihuan Li, Shiqi Lei; draft manuscript preparation: Zhihuan Li, Shiqi Lei, Kun Jiang; review: Yajuan Guo, Renmeng Liu, Lei Yang, Xingdan Wang, Yuheng Du. All authors reviewed and approved the final version of the manuscript.

Availability of Data and Materials: Data will be made available on request.

Ethics Approval: Not applicable.

Conflicts of Interest: The authors declare no conflicts of interest.

References

1. Kubes P, Jenne C. Immune responses in the liver. Annu Rev Immunol. 2018;36:247–77. doi:10.1146/annurev-immunol-051116-052415.
2. Tilg H, Adolph TE, Tacke F. Therapeutic modulation of the liver immune microenvironment. Hepatology. 2023;78(5):1581–601. doi:10.1097/hep.0000000000000386.
3. Yuan H, Xu R, Li S, Zheng M, Tong Q, Xiang M, et al. The malignant transformation of viral hepatitis to hepatocellular carcinoma: mechanisms and interventions. MedComm. 2025;6(3):e70121. doi:10.1002/mco2.70121.
4. Salimian J, Vazifedust S, Mirzaei Nodooshan M, Esmaeili Gouvarchinghaleh H. Natural products in the treatment of autoimmune hepatitis: a comprehensive review of therapeutic potential and mechanisms. Int Immunopharmacol. 2025;164:115366. doi:10.1016/j.intimp.2025.115366.
5. Beringer A, Thiam N, Molle J, Bartosch B, Miossec P. Synergistic effect of interleukin-17 and tumour necrosis factor-α on inflammatory response in hepatocytes through interleukin-6-dependent and independent pathways. Clin Exp Immunol. 2018;193(2):221–33. doi:10.1111/cei.13140.
6. Song R, Yu S, Chen X, Ling N, Cai D, Ren H, et al. Activation of the Jak2/Stat3 pathway by ROS-dependent signaling cascades initiates hepatitis B virus-induced hepatic inflammatory responses. Genes Dis. 2026;13(5):101857. doi:10.1016/j.gendis.2025.101857.
7. Roca Suarez AA, Testoni B, Baumert TF, Lupberger J. Nucleic acid-induced signaling in chronic viral liver disease. Front Immunol. 2020;11:624034. doi:10.3389/fimmu.2020.624034.
8. Sano E, Kazaana A, Tadakuma H, Takei T, Yoshimura S, Hanashima Y, et al. Interleukin-6 sensitizes TNF-α and TRAIL/Apo2L dependent cell death through upregulation of death receptors in human cancer cells. Biochim Biophys Acta Mol Cell Res. 2021;1868(7):119037. doi:10.1016/j.bbamcr.2021.119037.
9. Böer U, Fennekohl A, Püschel GP. Sensitization by interleukin-6 of rat hepatocytes to tumor necrosis factor α-induced apoptosis. J Hepatol. 2003;38(6):728–35. doi:10.1016/s0168-8278(03)00090-4.
10. Mansouri A, Gattolliat CH, Asselah T. Mitochondrial dysfunction and signaling in chronic liver diseases. Gastroenterology. 2018;155(3):629–47. doi:10.1053/j.gastro.2018.06.083.

11. Smirnova OA, Ivanova ON, Mukhtarov F, Valuev-Elliston VT, Fedulov AP, Rubtsov PM, et al. Hepatitis delta virus antigens trigger oxidative stress, activate antioxidant Nrf2/ARE pathway, and induce unfolded protein response. Antioxidants. 2023;12(4):974. doi:10.3390/antiox12040974.
12. Banerjee P, Gaddam N, Chandler V, Chakraborty S. Oxidative stress–induced liver damage and remodeling of the liver vasculature. Am J Pathol. 2023;193(10):1400–14. doi:10.1016/j.ajpath.2023.06.002.
13. Eum HA, Billiar TR. TNF/TNF receptor 1-mediated apoptosis in hepatocytes. In: Wallach D, Kovalenko A, Feldmann M, editors. Advances in TNF family research. New York, NY, USA: Springer; 2011. p. 617–24. doi:10.1007/978-1-4419-6612-4_65.
14. Prockop DJ, Oh JY. Mesenchymal stem/stromal cells (MSCs): role as guardians of inflammation. Mol Ther. 2012;20(1):14–20. doi:10.1038/mt.2011.211.
15. Lan Z, Tan F, He J, Liu J, Lu M, Hu Z, et al. Curcumin-primed olfactory mucosa-derived mesenchymal stem cells mitigate cerebral ischemia/reperfusion injury-induced neuronal PANoptosis by modulating microglial polarization. Phytomedicine. 2024;129:155635. doi:10.1016/j.phymed.2024.155635.
16. Shen P, Huang K, Zhang X, Yin G, Qin M, Ma H, et al. Genetically engineered MSC-derived hybrid cellular vesicles for ROS-scavenging and mitochondrial homeostasis in hepatic ischemia-reperfusion injury. Mater Today Bio. 2025;34:102215. doi:10.1016/j.mtbio.2025.102215.
17. Bruno S, Deregibus MC, Camussi G. The secretome of mesenchymal stromal cells: role of extracellular vesicles in immunomodulation. Immunol Lett. 2015;168(2):154–8. doi:10.1016/j.imlet.2015.06.007.
18. Harrell CR, Djonov V, Volarevic V. The cross-talk between mesenchymal stem cells and immune cells in tissue repair and regeneration. Int J Mol Sci. 2021;22(5):2472. doi:10.3390/ijms22052472.
19. Koch DW, Schnabel LV, Ellis IM, Bates RE, Berglund AK. TGF-β2 enhances expression of equine bone marrow-derived mesenchymal stem cell paracrine factors with known associations to tendon healing. Stem Cell Res Ther. 2022;13(1):477. doi:10.1186/s13287-022-03172-9.
20. Molaei S, Amiri F, Salimi R, Ferdowsi S, Bahadori M. Therapeutic effects of mesenchymal stem cells-conditioned medium derived from suspension cultivation or silymarin on liver failure mice. Mol Biol Rep. 2022;49(11):10315–25. doi:10.1007/s11033-022-07785-4.
21. Wang YC, Ding S, Wang YF, Xie H, Shan SL, Chen HW, et al. A potential approach of mesenchymal stem cells combined silybin for synergistic treatment in rheumatoid arthritis via ICOS/ICOSL. MedComm. 2025;6(11):e70450. doi:10.1002/mco2.70450.
22. Amin MM, Arbid MS. Estimation of the novel antipyretic, anti-inflammatory, antinociceptive and antihyperlipidemic effects of silymarin in Albino rats and mice. Asian Pac J Trop Biomed. 2015;5(8):619–23. doi:10.1016/j.apjtb.2015.05.009.
23. Abenavoli L, Capasso R, Milic N, Capasso F. Milk thistle in liver diseases: past, present, future. Phytother Res. 2010;24(10):1423–32. doi:10.1002/ptr.3207.
24. Mai M, Wang Y, Luo M, Li Z, Wang D, Ruan Y, et al. Silibinin ameliorates deoxycholic acid-induced pyroptosis in steatotic HepG2 cells by inhibiting NLRP3 inflammasome activation. Biochem Biophys Rep. 2023;35:101545. doi:10.1016/j.bbrep.2023.101545.
25. Ou Q, Weng Y, Wang S, Zhao Y, Zhang F, Zhou J, et al. Silybin alleviates hepatic steatosis and fibrosis in NASH mice by inhibiting oxidative stress and involvement with the nf-κB pathway. Dig Dis Sci. 2018;63(12):3398–408. doi:10.1007/s10620-018-5268-0.
26. van Velthoven CTJ, Rando TA. Stem cell quiescence: dynamism, restraint, and cellular idling. Cell Stem Cell. 2019;24(2):213–25. doi:10.1016/j.stem.2019.01.001.
27. Lavi Arab F, Yousefi F, Reza Jaafari M, Rajabian A, Dana H, Tabasi N, et al. Evaluation of the immune-modulatory, anti-oxidant, proliferative, and anti-apoptotic effects of nano-silymarin on mesenchymal stem cells isolated from multiple sclerosis patients' adipose tissue sources. J Funct Foods. 2024;113:105958. doi:10.1016/j.jff.2023.105958.
28. Aithal AP, Bairy LK, Seetharam RN, Kumar N. Hepatoprotective effect of bone marrow-derived mesenchymal stromal cells in CCl_4-induced liver cirrhosis. 3 Biotech. 2021;11(2):107. doi:10.1007/s13205-021-02640-y.

29. Makouie S, Bryś J, Małajowicz J, Koczoń P, Siol M, Palani BK, et al. A comprehensive review of silymarin extraction and liposomal encapsulation techniques for potential applications in food. Appl Sci. 2024;14(18):8477. doi:10.3390/app14188477.
30. Tang H, Luo H, Zhang Z, Yang D. Mesenchymal stem cell-derived apoptotic bodies: biological functions and therapeutic potential. Cells. 2022;11(23):3879. doi:10.3390/cells11233879.
31. Christoffers S, Seiler L, Wiebe E, Blume C. Possibilities and efficiency of *MSC* co-transfection for gene therapy. Stem Cell Res Ther. 2024;15(1):150. doi:10.1186/s13287-024-03757-6.
32. Preda MB, Neculachi CA, Fenyo IM, Vacaru AM, Publik MA, Simionescu M, et al. Short lifespan of syngeneic transplanted MSC is a consequence of *in vivo* apoptosis and immune cell recruitment in mice. Cell Death Dis. 2021;12:566. doi:10.1038/s41419-021-03839-w.
33. Zriek F, di Battista JA, Alaaeddine N. Mesenchymal stromal cell secretome: immunomodulation, tissue repair and effects on neurodegenerative conditions. Curr Stem Cell Res Ther. 2021;16(6):656–69. doi:10.2174/1574888X16666210202145639.
34. Seo Y, Kang MJ, Kim HS. Strategies to potentiate paracrine therapeutic efficacy of mesenchymal stem cells in inflammatory diseases. Int J Mol Sci. 2021;22(7):3397. doi:10.3390/ijms22073397.
35. Carter K, Lee HJ, Na KS, Fernandes-Cunha GM, Blanco IJ, Djalilian A, et al. Characterizing the impact of 2D and 3D culture conditions on the therapeutic effects of human mesenchymal stem cell secretome on corneal wound healing *in vitro* and *ex vivo*. Acta Biomater. 2019;99:247–57. doi:10.1016/j.actbio.2019.09.022.
36. Sánchez-Rodríguez VH, Pérez-Cortez JE, Gallegos-Martínez S, Chuck-Hernández C, Rodriguez CA, Boccaccini AR, et al. Light-based and cost-effective bioprinting of musculoskeletal GelMA constructs enriched with mesoporous bioactive glass nanoparticles. Int J Bioprinting. 2024;10(4):1830. doi:10.36922/ijb.1830.
37. Damiri F, Simińska-Stanny J, Rasoulian F, Pinal C, Kaczmarek-Szczepanska B, Patel CD, et al. Emerging trends in polysaccharide-based smart PEGylated hydrogels for biomedical applications. Carbohydr Polym. 2026;375:124707. doi:10.1016/j.carbpol.2025.124707.
38. Lin CH, Srioudom JR, Sun W, Xing M, Yan S, Yu L, et al. The use of hydrogel microspheres as cell and drug delivery carriers for bone, cartilage, and soft tissue regeneration. Biomater Transl. 2024;5(3):236–56. doi:10.12336/biomatertransl.2024.03.003.
39. Si H, Chen Y, Jiang K, Ma K, Ramsey E, Oakey J, et al. Deterministic single-cell encapsulation in PEG norbornene microgels for promoting anti-inflammatory response and therapeutic delivery of mesenchymal stromal cells. Adv Healthc Mater. 2024;13(14):e2304386. doi:10.1002/adhm.202304386.
40. Ge Z, Wang C, Tao Y, Qiu F, Liu F, Guo W, et al. Dual-layer flexible liquid metal fiber for plantar pressure monitoring and synchronous wound electrotherapy. Adv Healthc Mater. 2026;15(1):e02681. doi:10.1002/adhm.202502681.
41. Hoyle C, Bowman C. Thiol–ene click chemistry. Angew Chem Int Ed. 2010;49(9):1540–73. doi:10.1002/anie.200903924.
42. Jiang Z, Shaha R, Jiang K, McBride R, Frick C, Oakey J. Composite hydrogels with controlled degradation in 3D printed scaffolds. IEEE Trans NanoBioscience. 2019;18(2):261–4. doi:10.1109/TNB.2019.2905510.
43. Jiang Z, Xia B, McBride R, Oakey J. A microfluidic-based cell encapsulation platform to achieve high long-term cell viability in photopolymerized PEGNB hydrogel microspheres. J Mater Chem B. 2017;5(1):173–80. doi:10.1039/C6TB02551J.
44. Contessi Negrini N, Sun H, Celiz AD. Tailoring composite hydrogel performance via controlled integration of norbornene-functionalised Pluronic micelles. Biomater Sci. 2026;14(2):518–30. doi:10.1039/d5bm01434d.
45. Kirkpatrick BE, Dhand AP, Hibbard LP, Jaeschke MW, Yendamuri T, Nelson BR, et al. Ultrafast-relaxing and photopolymerizable PEG hydrogels enable viscoelasticity-mediated cell remodeling in synthetic matrices. Matter. 2026;9(2):102524. doi:10.1016/j.matt.2025.102524.
46. Jiang Z, Shaha R, McBride R, Jiang K, Tang M, Xu B, et al. Crosslinker length dictates step-growth hydrogel network formation dynamics and allows rapid on-chip photoencapsulation. Biofabrication. 2020;12(3):035006. doi:10.1088/1758-5090/ab7ef4.

47. Jiang Z, Jiang K, Si H, McBride R, Kisiday J, Oakey J. One step encapsulation of mesenchymal stromal cells in PEG norbornene microgels for therapeutic actions. ACS Biomater Sci Eng. 2023;9(11):6322–32. doi:10.1021/acsbiomaterials.3c01057.
48. Jiang K, Zhou S, Li Z, Guo Y, Lei S, Wang X, et al. Droplet-microfluidic-assisted high throughput fabrication of microgels supports assembly of spheroid-like structures and promotes survival and glucose sensitivity of encapsulated β-cells. Appl Mater Today. 2026;48:103035. doi:10.1016/j.apmt.2025.103035.
49. Frahm E, Lin CC. Dynamic granular hydrogels to assess pancreatic cancer cell fate. Biomater Sci. 2026;14(6):1488–99. doi:10.1039/d5bm00997a.
50. Elgazar AA, Selim NM, Abdel-Hamid NM, El-Magd MA, El Hefnawy HM. Isolates from *Alpinia officinarum* Hance attenuate LPS-induced inflammation in HepG2: evidence from *in silico* and *in vitro* studies. Phytother Res. 2018;32(7):1273–88. doi:10.1002/ptr.6056.
51. Zeng J, Du S, Zhou J, Huang K. Role of SelS in lipopolysaccharide-induced inflammatory response in hepatoma HepG2 cells. Arch Biochem Biophys. 2008;478(1):1–6. doi:10.1016/j.abb.2008.07.016.
52. Pierdomenico M, Riccioni C, Benassi B. Anti-inflammatory effect of a pomegranate extract on LPS-stimulated HepG2 cells. Nat Prod Res. 2024;38(5):727–34. doi:10.1080/14786419.2023.2196622.
53. Gutiérrez-Ruiz MC, Quiroz SC, Souza V, Bucio L, Hernández E, Olivares IP, et al. Cytokines, growth factors, and oxidative stress in HepG2 cells treated with ethanol, acetaldehyde, and LPS. Toxicology. 1999;134(2–3):197–207. doi:10.1016/s0300-483x(99)00044-x.
54. Hu X, Wang Y, Xu M. Study of the cell responses in tantalum carbide nanoparticles-enriched polysaccharide composite hydrogel. Int J Biol Macromol. 2019;135:501–11. doi:10.1016/j.ijbiomac.2019.05.191.
55. Widhe M, Bysell H, Nystedt S, Schenning I, Malmsten M, Johansson J, et al. Recombinant spider silk as matrices for cell culture. Biomaterials. 2010;31(36):9575–85. doi:10.1016/j.biomaterials.2010.08.061.
56. Helen W, Gough JE. Cell viability, proliferation and extracellular matrix production of human annulus fibrosus cells cultured within PDLLA/Bioglass composite foam scaffolds *in vitro*. Acta Biomater. 2008;4(2):230–43. doi:10.1016/j.actbio.2007.09.010.